Atmos. Meas. Tech., 9, 1207–1219, 2016
www.atmos-meas-tech.net/9/1207/2016/
doi:10.5194/amt-9-1207-2016

Atmospheric Measurement Techniques
Open Access
EGU

Intercomparison of in situ water vapor balloon-borne measurements from Pico-SDLA H_2O and FLASH-B in the tropical UTLS

Mélanie Ghysels[1,a], Emmanuel D. Riviere[1], Sergey Khaykin[2], Clara Stoeffler[1], Nadir Amarouche[3], Jean-Pierre Pommereau[2], Gerhard Held[4], and Georges Durry[1]

[1]Groupe de Spectrométrie Moléculaire et Atmosphérique, UMR CNRS 7331, UFR Sciences Exactes et Naturelles, Moulin de la Housse, BP 1039, 51687 Reims CEDEX 2, France
[2]LATMOS, CNRS, Université de Versailles St. Quentin, Guyancourt, France
[3]Division technique de l'Institut National des Sciences de l'Univers,
Place Aristide Briand, 92195 Meudon CEDEX 1, France
[4]Instituto de Pesquisas Meteorológicas (IPMet)/ Universidad e Estadual Paulista (UNESP),
CX Postal 281, 17015-970 Bauru, São Paulo, Brazil
[a]now at: National Institute of Standards and Technology, Gaithersburg, MD, USA

Correspondence to: Mélanie Ghysels (melanie.ghysels@nist.gov)

Received: 10 November 2015 – Published in Atmos. Meas. Tech. Discuss.: 21 December 2015
Revised: 17 February 2016 – Accepted: 3 March 2016 – Published: 21 March 2016

Abstract. In this paper we compare water vapor mixing ratio measurements from two quasi-parallel flights of the Pico-SDLA H_2O and FLASH-B hygrometers. The measurements were made on 10 February 2013 and 13 March 2012, respectively, in the tropics near Bauru, São Paulo state, Brazil during an intense convective period. Both flights were performed as part of a French scientific project, TRO-Pico, to study the impact of the deep-convection overshoot on the water budget. Only a few instruments that permit the frequent sounding of stratospheric water vapor can be flown within small-volume weather balloons. Technical difficulties preclude the accurate measurement of stratospheric water vapor with conventional in situ techniques. The instruments described here are simple and lightweight, which permits their low-cost deployment by non-specialists aboard a small weather balloon. We obtain mixing ratio retrievals which agree above the cold-point tropopause to within 1.9 and 0.5 % for the first and second flights, respectively. This level of agreement for balloon-borne measured stratospheric water mixing ratio constitutes one of the best agreement reported in the literature. Because both instruments show similar profiles within their combined uncertainties, we conclude that the Pico-SDLA H_2O and FLASH-B data sets are mutually consistent.

1 Introduction

Water vapor in the stratosphere plays an important role in the radiative and chemical budget (Shindell et al., 1998; Herman et al., 2002; Loewenstein et al., 2002). Changes in the stratospheric humidity can have a significant impact on the climate and the radiative balance of the Earth atmosphere (Forster and Shine, 2002; Solomon et al., 2010; Riese et al., 2012). Climate models show that an increase in stratospheric humidity can lead to stratospheric cooling and consequently to a more important ozone depletion (Shindell, 2001; Dvorstov and Solomon, 2001).

Regular radiosonde measurements are reliable only in the lower-to-middle troposphere zone, whereas high-precision hygrometers must be employed for stratospheric measurements because this region is so dry. Although a variety of techniques have been developed for measuring water vapor in the stratosphere, achieving high-accuracy measurements of humidity in the stratosphere is far from routine. Current stratospheric measurements of humidity include frost-point detection, light absorption using tunable diode laser spectrometers and fluorescence (Lyman-α radiation) methods. Usually, in situ instruments have a higher precision and a better spatial resolution than remote sensing instruments because the former measurements are performed directly in-

side the air mass and do not require geophysical inversion. Several balloon-borne measurements to monitor the stratospheric water vapor have been conducted since the early 1980s (Kley et al., 2000; Oltmans et al., 2000; Rosenlof et al., 2001; Vömel et al., 2002, 2007a, b; Jensen et al., 2005, 2008; Read et al., 2007; Weinstock et al., 2009; Hurst et al., 2011; Berthet et al., 2013; Rollins et al., 2014; Kindel et al., 2015). In some cases, coincident flights have been realized leading to comparisons of in situ water vapor measurements (Jensen et al., 2005, 2008; Vömel et al., 2007a, b; Weinstock et al., 2009; Hurst et al., 2011; Berthet et al., 2013). However, persistent disagreements remain. For example, Vömel et al. (2007a) compared in situ balloon-borne measurements of water vapor from several instruments during coincident flights. Comparison of in situ water vapor measurements from the CFH (cryogenic frost-point hygrometer) and the NOAA/CSD aircraft hygrometer (cryogenic frost-point hygrometer) led to differences ranging up to 40 % between 14 and 17 km. Throughout the entire altitude range (from 10 to 20 km) the measurements from the Harvard Lyman-α hygrometer and the CFH showed considerable discrepancies up to 110 %. Differences of $\pm$10 % were found by comparing the FLASH-B (Lyman-α) and NOAA/CMDL (frost-point hygrometer) water vapor measurements obtained at altitudes of 15 km, in the polar stratosphere (Vömel et al., 2007b). Jensen et al. (2008) found that discrepancies between nearly simultaneous water vapor measurements in the TTL (tropical tropopause layer) could reach 2 to 3 ppmv: this latter work compares measurements from the Harvard water vapor instrument (HWV, Lyman-α) and from the Harvard ICOS (integrated cavity output spectroscopy) instrument within the altitude range 15 to 19 km. More generally, in the TTL the measurements have shown discrepancies larger than 10 %. The main problem for in situ measurements of water vapor is contamination by outgassing from the balloon and the instrument structure. Recently, the proper selection of wall materials and the judicious positioning of the different elements have significantly reduced this confounding effect.

The TRO-Pico project, which is funded by the French National Research Agency (ANR) for 5 years, was launched in 2010. The main objectives of TRO-Pico are to combine balloon-, ground-, and satellite-based observations as well as model simulations at different scales to study the impact of deep-convection overshoots on the stratospheric humidity. The balloon campaigns were realized during March 2012 and from November 2012 to March 2013 in Bauru, São Paulo state, Brazil, and were hosted by IPMet (Instituto de Pesquisas Meteorológicas). The campaigns were divided into two periods: the SMOP (6-month observation period) to study the change of water vapor during the overall convective season and the IOP campaign (intensive observation period), occurring during the most intense convective period, to study the troposphere-to-stratosphere transport and the stratospheric moistening impact. Both comparison flights discussed here are part of the IOP. Within both periods, 31 successful water vapor flights were carried out under small zero-pressure balloons from 500 to 1500 m^3, or 1.2 kg rubber balloons. Water vapor measurements were performed using two lightweight hygrometers: Pico-SDLA H_2O and FLASH-B. A forthcoming paper will present the meteorological/dynamical analysis of the water vapor measurements linked to specific hydration in the lower stratosphere (Khaykin et al., 2013b).

In order to validate the observations, Pico-SDLA and FLASH were launched twice on the same day within a 3 h interval close to the convection overshoot event: 13 March 2012 and 10 February 2013. These two cases will be discussed in this paper. These flights were performed using small weather balloons in order to limit the effect of water outgassing. Only a few instruments can be flown under such small-volume balloons to permit regular soundings. Unlike other compact hygrometers where the speed of descent prevents accurate measurements, these instruments can measure stratospheric water vapor even during descent under parachutes.

The purpose of this study is to evaluate the accuracy of the water vapor measurements preformed during this campaign and to quantify the consistency of the data produced by the two hygrometers. Both Pico-SDLA and FLASH hygrometers are described in the Sect. 2 and the flight train is described in Sect. 3. The in situ water vapor measurements in the TTL and lower stratosphere are compared for each of the flights in the Sect. 4.

2 Instrumentation

2.1 The Pico-SDLA H_2O hygrometer

2.1.1 Description of Pico-SDLA H_2O

Pico-SDLA H_2O (hereafter Pico-SDLA) is a lightweight spectrometer which measures water vapor using laser absorption spectroscopy (Durry et al., 2008). The probe laser emits at a wavelength of 2.63 µm and has a 1 m path length through ambient air. This hygrometer was flown during a coincident flight with the ELHYSA frost-point hygrometer in March 2011, leading to a stratospheric water vapor measurement comparison (Berthet et al., 2013). Both hygrometers agreed to within 3.5 % in the polar stratosphere, which is well below their combined instrumental uncertainties.

The mass of the Pico-SDLA is less than 9 kg, making it suitable as a payload for small stratospheric balloons (500 and 1500 m^3). Its design was improved in 2012 in order to meet the requirements of TRO-Pico campaigns. The electronic components are now integrated into a Rohacell box on the top of the cell, which makes the instrument more compact. Figure 1 shows the new version of the hygrometer. It uses a distributed feedback diode laser emitting at 2.63 µm. This diode has temperature and current controls. Then, we distinguish the current modulation from the TEC temperature

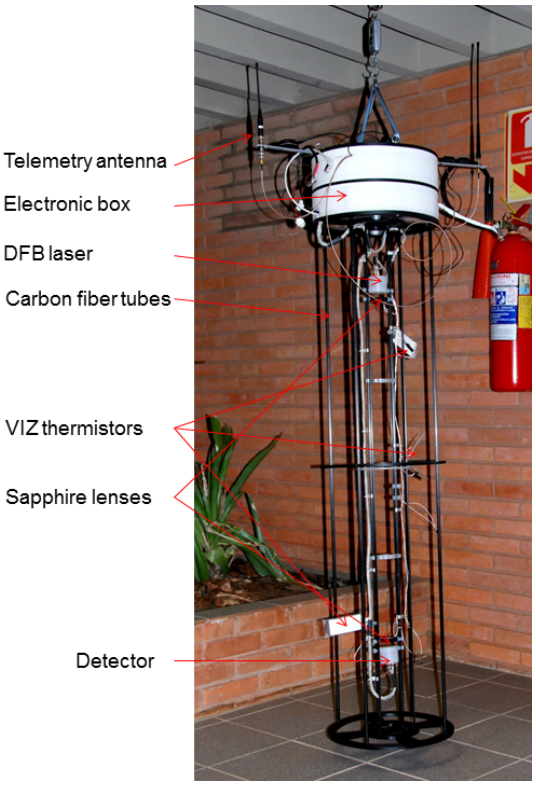

Figure 1. Description of the Pico-SDLA H_2O hygrometer, improved for the TRO-Pico campaign (2012–2013).

tuning. The current modulation of the laser is the preferred method to scan the water vapor absorption line since the response time is much faster than for a TEC temperature modulation; the water vapor absorption line is scanned by tuning the laser current and fixing the TEC temperature. After passing through the ambient-air sample, the laser beam is focused onto an indium arsenide detector using a sapphire lens. The mechanical structure of the sensor comprises carbon fiber tubes to strengthen the overall instrument, especially for the landing with parachutes. The instrument is equipped with a TM/TC antenna to transmit the spectrum data to the ground during the flight and to control instrument parameters in case intervention is required. The sensor is able to measure water vapor from the ground to altitudes of 35 km for concentrations ranging from 15 000 ppmv to less than 1 ppmv.

Two different rotation–vibration absorption transitions of water vapor are probed because of the large variation in mixing ratio occurring between the troposphere and the stratosphere. For measurements from the ground to around 200 hPa pressure level, we used the $4_{13} \leftarrow 4_{14}$ $H_2^{16}O$ line at 3802.96561 cm^{-1}. Above 200 hPa pressure level, we use the $2_{02} \leftarrow 1_{01}$ $H_2^{16}O$ line at 3801.41863 cm^{-1}. During in-flight measurements, the switch from one line to the other is automatically driven. Both sets of line parameters are obtained from HITRAN 2012 database (Rothman et al., 2013). In HITRAN, the line intensities for these two lines are based on the work by R. A. Toth at JPL (Jet Propulsion Laboratory, NASA) with a relative uncertainty of 2 % (see "Linelist of water vapor parameters from 500 to 8000 cm^{-1}" at http://mark4sun.jpl.nasa.gov/h2o.html). The water vapor transition is determined prior to the launch, thus allowing for automatic selection during in-flight measurements.

The mixing ratio is extracted from the measured spectra using a nonlinear least squares fitting algorithm applied to the measured line shape. We use the Beer–Lambert law to model the spectrum and use a Voigt profile (VP) to describe the molecular line shape. In the case of the VP, the self- and air-broadening effects are taken into account. In HITRAN 2012, for the two lines, the self-broadening uncertainty is ±5–10 % and the air-broadening uncertainty is ±2–5 %. We conducted some tests to determine the impact of the width uncertainties on the retrieved mixing ratio; they induced an error smaller than 1 %. We found that fitting the VP to the measured spectra yielded residuals consistent with the instrument noise. No evidence of systematic residuals caused by higher-order line shape effects was observed for stratospheric pressures (our region of interest). Figure 2 shows an example of the transmission of three atmospheric spectra of the H_2O $2_{02} \leftarrow 1_{01}$ line recorded during the 10 February 2013 flight in Bauru at different altitudes in the lower stratosphere (24.24 hPa ≡ 25.2 km; 73.60 hPa ≡ 18.4 km; 101.05 hPa ≡ 16.6 km). During this flight, the cold-point tropopause (hereafter CPT) altitude was approximately 16.7 km. In the upper panel, the black and red lines represent the measurement and fitted results, respectively. The corresponding fit residuals are shown in the bottom panel. The standard deviation of the residuals is around 2×10^{-4} and corresponds to the noise level of the measured beam transmission. These residuals do not show any W structure, which is observed when the VP is fitted to transitions exhibiting non-Voigt effects such as Dicke narrowing and/or speed-dependent effects (Dicke, 1953; Rautian and Sobel'man, 1967; Tran et al., 2007; Boone et al., 2007). Defining the spectrum signal-to-noise ratio (SNR) as the peak absorbance divided by the baseline standard deviation, we find a maximum SNR of approximately 65 : 1. For the relatively low pressures (20 to 120 hPa) and hence low absorbances encountered in the TTL and in the lower stratosphere the VP provides an accurate representation of the measured spectrum for the noise levels of this spectrometer. At higher pressures (in the troposphere) a more sophisticated line shape may be necessary because the spectrum SNR may reveal systematic deviations from the VP.

Several tests were conducted to determine the sensitivity of the fitting procedure to the baseline interpolation, as well as to the temperature and pressure measurement uncertainties. These tests were realized using a synthetic spectrum with a noise level equivalent to the in-flight spectra. Details of these tests are given below.

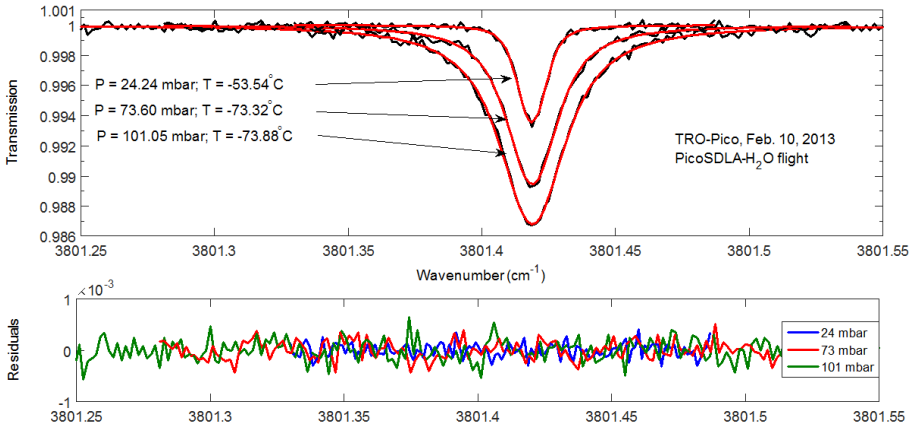

Figure 2. Transmission of the atmospheric spectra of the $2_{02} \leftarrow 1_{01}$ line of $H_2^{16}O$ from Pico-SDLA H_2O measurements on 10 February 2013 during the descent of the balloon. The top panel shows three experimental spectra (black line) and the results from fitting procedure (red line). These spectra were recorded at 25.2 km (24.24 mbar), 18.4 km (73.6 mbar) and 16.5 km (101.05 mbar) of altitude. The bottom panel shows the fit residuals for each spectrum.

The absorption spectrum is extracted from the atmospheric spectra by removing structure in the baseline which is induced by optical components and vibrations of the optical cell. The baseline is interpolated using a polynomial combined with a sinusoid term which takes into account commonly observed interference fringes caused by Fabry–Pérot effects between optics. The quality of the fitting procedure is influenced by the spectrum SNR, the polynomial order and the number of points chosen for the interpolation. The combined uncertainty introduced by these different factors varies with the peak absorbance of the line and consequently with the pressure level from 4.5 % at 50 hPa to 0.7 % at 150 hPa.

The air pressure is measured using a Honeywell absolute pressure transducer (model PPT0020AWN2VA) which operates between −40 °C and +85 °C with a manufacturer-specified relative uncertainty of 0.05 % full scale (0.7 hPa). The pressure measurements are corrected for drift caused by changes in temperature. During the TRO-Pico campaign flights, the atmospheric temperature ranged from −85 °C to +35 °C. In order to eliminate measurement error caused by being outside the instrument's temperature operating range, the pressure sensor is placed inside an enclosure having a minimum temperature of 0 °C. The uncertainty in the fitted water vapor concentration caused by temperature-dependent sensitivity of the pressure sensor is estimated to be ∼ 0.05 %.

The temperature is measured using three SIPPICAN thermistors which are coated to limit solar radiation effects. These sensors are located on each end and at the center of the optical cell, providing an average temperature for the measurements. The rotation of the optical cell during the flight induces a temperature difference between the three thermistors, which varies from 0 to 5 °C. This depends on the solar exposure of the thermistors (in the case of daytime flights). For this reason, we select the lowest measured temperature for the data processing. It has to be noted that the two measurements discussed in this paper were performed during nighttime, so this latter effect should not play a role here. Each sensor was calibrated independently by the manufacturer between −90 and +50 °C. The uncertainty of the temperature is specified to be 0.3 °C, yielding a 0.25 % uncertainty in the measured mixing ratio.

By taking into account all sources of error that we can estimate (i.e., spectroscopic and experimental errors as well as errors due to spectra processing), the combined relative standard uncertainty ranges from 7.5 % to 3.5 % in the TTL and the lower stratosphere, depending on the local conditions. Since temperature and pressure are input variables for the mixing ratio retrievals, we investigated the consistency of these measurements. We compared the Pico-SDLA measurements with those of a Vaisala RS-92 radiosonde during one coincident flight on 18 January 2013. Details of this work are provided in the next section.

2.1.2 Temperature and pressure measurement comparison on 18 January 2013

On 18 January, Pico-SDLA was launched at 22:11 UTC under a 1500 m^3 balloon. The time is recorded in UTC using a GPS-disciplined clock located on board the Pico-SDLA. One measurement is made every 300 to 500 ms depending on the SNR of the measurements and on the vertical speed of the payload during the flight. The measurements start as soon as they are requested by the operator, independently of launch time. The RS-92 radiosonde, attached to the same balloon, detects the launch time and records it as $t = 0$. Thereafter, it takes one measurement every 10 s.

The data were synchronized by applying a small temporal offset to the time stamps. This offset was determined from the cross-correlation of the temperature profiles from

both sensors and corresponded to the maximum of the cross-correlation.

We calculated the mean temperature difference (mean ΔT), the mean pressure difference (mean ΔP) as well as the standard deviations of the differences $\sigma(\Delta\mathrm{T})$ and $\sigma(\Delta P)$. We only used the ascent measurements for the comparison. It has to be noted that a part of the ascent was made during daytime. Although the descent of the Pico-SDLA occurs under parachute, this is not the case of the radiosonde which remains attached to the balloon. The vertical speeds of both sensors are consequently different therefore precluding correlation with time. Since only the descent measurements of Pico-SDLA are usable, the radiosonde is never attached to Pico-SDLA during this time. Indeed, the RS-92 telemetry system at 403 MHz induces a modulation of the laser emission, which creates two sidebands on the spectrum rendering them unusable.

The temperature uncertainty on the RS-92 is 0.5 °C while the pressure uncertainty is quoted by the manufacturer for two pressure ranges: 1080 to 100 hPa and 100 to 3 hPa, for which the combined standard uncertainty is 1.5 and 0.6 hPa, respectively.

Within the overall altitude range of the flight, the mean ΔT for this flight is 0.12 °C with a standard deviation $\sigma(\Delta T)$ of 0.28 °C. The mean ΔT is less than both uncertainties. The ΔT is always lower than 0.5 °C except above 23 km where the RS-92 exhibited large spikes in the measured temperature. Therefore, for this flight we concluded that the RS temperature was unreliable above this altitude. The SIPPICAN and the RS-92 measurements agree well with the observations of Nash et al. (2011) and Bower and Fitzgibbon (2004), which were obtained by comparing different types of temperature sensors. In these studies, the comparison of temperature measurements, using corrected data, led to temperature differences up to 0.4 °C during night flights and 1 °C for daytime flights. The differences are usually higher above the tropopause, which is probably due to icing of the sensor.

The mean pressure difference (mean ΔP) and the standard deviation of this difference $\sigma(\Delta P)$ are -0.024 and 0.163 hPa, respectively. This pressure difference is below the uncertainties of both the Pico-SDLA and RS-92 pressure sensors. Between the ground and 2.6 km, the pressure differences are as large as 0.5 hPa. This behavior was also observed in the 8th WMO High Quality Radiosonde Intercomparison (Nash et al., 2011). During this campaign, the performance of radiosonde systems' pressure measurements was investigated. It was found that the pressure differences ranged from 0 to 1.4 hPa and correlated with the altitude of the balloon. The biggest differences occurred near the ground.

We determined the consistency of measurement pairs using the GRUAN (Reference Upper-Air Network) analysis approach detailed by Immler et al. (2010). Given two independent measurements, m_1 and m_2, and their respective uncertainties, u_1 and u_2, these two measurements can be considered consistent if $|m_1 - m_2| < k\sqrt{u_1^2 + u_2^2}$. Here, k is the statistical significance factor. For $k = 1$, if the condition is true, the measurements are consistent.

For measurements of temperature and taking into account each sensor uncertainty, we find that $k\sqrt{u_1^2 + u_2^2} = 0.58$. Thus, to be consistent, the measurements of absolute difference, expressed as $|m_1 - m_2|$, must be lower than 0.58. The mean temperature difference, calculated from in situ measurements, is 0.05 ± 0.15 °C. Likewise for pressure, the mean ΔP has to be less than 0.92 hPa. In our case, the mean pressure difference is (0.02 ± 0.11) hPa. For both parameters, the condition is satisfied and, therefore, the measurements are consistent following the GRUAN approach.

2.1.3 Water vapor outgassing

Contamination of water vapor measurements caused by outgassing from the balloon envelope or instrument surfaces was first observed in the in situ measurements of Mastenbrook (1968) and Zander (1966). For the TRO-Pico campaign, the use of small-volume weather balloons (1500 or 500 m^3) is expected to reduce the water vapor outgassing from the balloon envelope. We found that the ascent mixing ratio reached as high as 25 ppmv, whereas the mean stratospheric mixing ratio was 4 ppmv. Therefore, we used only the measurements obtained during descent. We compared these measurements from Pico-SDLA with those of FLASH-B to determine whether or not outgassing of water vapor contaminated the data. As described in detail in the following section, we found that the FLASH-B descent measurements did not suffer from outgassing contamination. During the beginning of the descent, a small contamination (up to 0.5 ppmv and visible up to 3 km in average below the float altitude) of the Pico-SDLA data was observed. Therefore, we considered the Pico-SDLA data below the altitude where the contamination is observed.

2.2 The FLASH-B hygrometer

The balloon version of FLASH is a compact lightweight sonde developed at the Central Aerological Observatory, Russia, for balloon-borne water vapor measurements in the upper troposphere and stratosphere (Yushkov et al., 1998). The instrument is based on the fluorescent method (Kley and Stone, 1978; Bertaux and Delannoy, 1978), which uses the photodissociation of H_2O molecules exposed to vacuum ultraviolet radiation ($\lambda < 137$ nm) followed by the measurement of the fluorescence of excited OH radicals using a Hamamatsu photomultiplier in photon-counting mode. The intensity of the fluorescent light sensed by the photomultiplier is directly proportional to the water vapor mixing ratio under stratospheric conditions (10–150 hPa). The H_2O measurement range is limited to pressures lower than 300 hPa because of strong Lyman-α absorption in the lower troposphere. The instrument uses an open optical layout, where

the analyzed volume is located outside the instrument. This design allows reduction of the instrument size to that of a small sonde with a total mass (including batteries) of about 1 kg. This arrangement restricts the use of the instrument to nighttime only.

Each FLASH-B instrument is calibrated in the laboratory against a reference dew-point hygrometer, MBW 373L. A description of the procedure can be found in Vömel et al. (2007b). The detection limit for a 4 s integration time at stratospheric conditions is approximately 0.1 ppmv, while the accuracy is limited by the calibration error amounting to a relative uncertainty of 4 %. The typical measurement precision in the stratosphere is 5 to 6 %, whereas the combined relative uncertainty in water vapor concentration is less than 10 % throughout the stratosphere. The FLASH-B has been successfully used in a number of balloon campaigns (e.g., LAUTLOS-WAVVAP, SCOUT-AMMA, TC4, LAPBIAT-II) which included simultaneous measurements of stratospheric water vapor by different measurement techniques. In particular, point-by-point comparison with the frost-point hygrometer from the NOAA/CMDL showed a mean deviation of 2.4 with 3.1 % standard deviation (1σ) (Vömel et al., 2007a), and comparison with CFH showed a mean deviation of 0.8 % with a 4 % relative standard deviation (Khaykin et al., 2013a).

The flight configuration of the FLASH-B, in which the analyzed volume is located beneath the downward-looking optics 2–3 cm away from the lens, caused noticeable self-contamination during balloon ascent because of water outgassing from the instrument surfaces and balloon. The contamination effect is observed as a quasi-exponential growth of water vapor readings above about 70 hPa level during the ascent. This occurs because the relative contribution of water carried on the sounding equipment surfaces becomes more significant as the number density of ambient water molecules decreases with altitude. In contrast, the FLASH-B measurements during the descent at the bottom of the flight train in undisturbed air are free of contamination as shown by the reduction in water vapor readings immediately after the burst of balloon. Here we use the contamination-free descent profiles along with the clean ascent profiles below 75 hPa.

3 Balloon flight trains

The flights have been realized under small zero-pressure balloons of 500 and 1500 m^3 volume for Pico-SDLA instruments and 1.2 kg rubber balloons for the FLASH instruments. The launch of these balloons was realized by the French scientific team, assisted by staff from IPMet.

During the SMOP, regular soundings of the upper troposphere/lower stratosphere using the Pico-SDLA H_2O spectrometer were conducted by the technicians of IPMet without the presence of the French scientific teams. The hygrometer operation was simplified to permit its deployment by non-specialists. During this period, the hygrometer was deployed under 500 m^3 zero-pressure Aerostar balloons.

For all flights, the flight train includes a parachute, a cutter device and a balloon telemetry/remote control system (E-track iridium), a strobe light and a radar reflector. The cutter device is used to separate the payload from the balloon, with the payload descending under the parachute. The E-track iridium allows one to follow the flight train during the ascent and the descent and to initiate separation from the balloon. The scientific instrument is connected to the flight train by a nylon rope. The flight trains were easy to implement and permitted quick deployment of the instruments with respect to larger balloons.

For the water vapor flights of Pico-SDLA, the instrument was located at least 15 m below the balloon to limit outgassing from the balloon envelope. On 13 March 2012, the instruments of the flight train, from bottom to top, were the Pico-SDLA H_2O, and the LOAC Optical Particle Counter (Renard et al., 2015). The total payload weight for this flight was 15 kg under a 500 m^3 balloon. On 10 February 2013, the instruments of the flight train, from bottom to top, were the Pico-SDLA H_2O and the Pico-SDLA CH_4 (Ghysels et al., 2011). The total payload mass was 25 kg under a 1500 m^3 balloon.

For flights of the FLASH-B, the E-track box and cutter device were not included in the flight train. The instruments of the flight train were, from bottom to top, the FLASH-B and the COBALD (Compact Optical Backscatter and Aerosol Detector) backscatter sonde (Brabec et al., 2012) on 13 March 2012 and FLASH-B, COBALD and LOAC on 11 February 2013. The overall payload masses were 7.4 and 9.4 kg, respectively.

4 Comparison of mixing ratio retrievals

4.1 Flight conditions

The flights of 10–11 February 2013 and 13 March 2012 were intended to capture the signature of the overshoots in water vapor profiles. The launch site was located on the UNESP Bauru Campus, at the outskirts of town (coordinates: 22.36° S, 49.03° W).

On 10 February 2013, the Pico-SDLA was launched at 21:03 UTC with overshooting conditions observed by the IPMet S band radar located 200 km east of Bauru. Subsequently, a convective cell reached an altitude of > 16 km, which was about 150 km east of the launch site position. On this day, the most intense convective events occurred between 18:06 and 21:15 UTC. The FLASH-B hygrometer was launched at 00:09 UTC, 3 h later than Pico-SDLA.

On 13 March 2012, Pico-SDLA H_2O was launched at 19:20 UTC in convective conditions and FLASH-B was launched 3 h later. On this day, strong convection was observed until 21:00 UTC east and southeast of Bauru with convective cells reaching altitudes exceeding 18 km. Both instru-

ments were able to catch the signature of an overshooting cell reaching 19.2 km.

During the descent, the vertical speed of the instruments ranged from 60 m s^{-1} (just after the flight train separates from the balloon) to 20 m s^{-1} in the TTL. In this condition, the Pico-SDLA spectra were recorded without any averaging or a maximum average of five spectra in order to achieve good vertical resolution and to avoid excessive overlapping of mixing ratio measurements from different layers of the TTL.

4.2 13 March 2012 flight

Figure 3 shows the trajectory plot for Pico-SDLA and FLASH flights on 13 March 2012. The altitude of the trajectories is color-coded and the time is in UTC. Altitudes between 15 and 28 km are considered, representing the TTL and lower stratosphere, which are our regions of interest. Pico-SDLA flew 22 km to the west of FLASH. The ascent of Pico-SDLA lasted 1 h 49 min followed by a float of 14 min at 23.6 km (30.5 hPa) before a 40 min long descent. The ascent of FLASH-B lasted 1 h 15 min followed by a descent of 1 h 12 min. The maximum altitude reached by FLASH was 21.6 km (45 hPa).

The comparison of water vapor mixing ratio profiles from FLASH and Pico-SDLA between 21.3 km (44.5 hPa) and 15 km (131 hPa) is shown in Fig. 4. Up to 21.3 km, Pico-SDLA measurements do not show any outgassing effects. In this figure, the CPT altitude from Pico-SDLA (orange dashed line) and FLASH (brown dashed line) is located at 17.95 km (78.5 hPa) and 17.44 km (86.6 hPa), respectively. The CPT altitude of each instrument is determined from the descent temperature profiles. This altitude corresponds to the level of the minimum temperature and has an important role in the troposphere-to-stratosphere coupling and exchange. The water vapor transport from the troposphere to the stratosphere is partially dependent on the thermal characteristics of the CPT (Holton et al., 1995; Mote et al., 1996; Kim and Son, 2012; Randel and Jensen, 2013). The lower boundary of the TTL is defined in Fueglistaler et al. (2009) as the area above the level of the mean convective outflow ($\sim$ 14 km). The upper boundary is set at 70 hPa (18.6 km), above which the atmosphere is governed mainly by stratospheric processes (green dash line in Fig. 4). The temperature profiles are also shown in orange and brown lines. The CPT is much colder in this case than for the 10 February flight ($-79\,^{\circ}$C in average instead of $-74.6\,^{\circ}$C).

The RS-92, integrated into FLASH, measures the geopotential altitude whereas the GPS on board Pico-SDLA measures the geometric altitude, inducing a shift of 378 m in altitude. To correct for this difference, we used the altitude measurements from the COBALD sonde, which are obtained from a GPS. Thus, we were able to reconstruct the FLASH altitude scale by interpolating the COBALD data with respect to the time into flight. The same operation has been

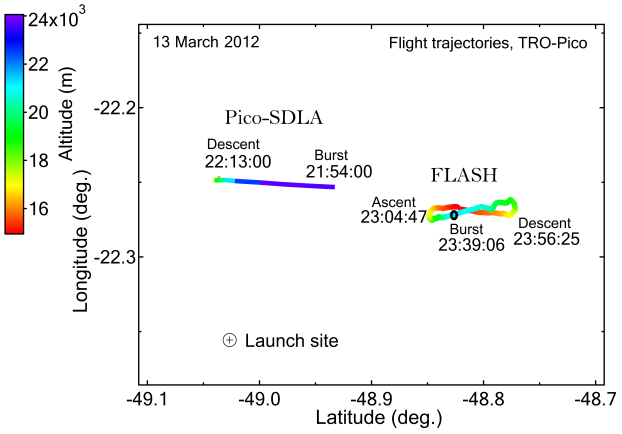

Figure 3. Balloon trajectories of Pico-SDLA and FLASH flights on 13 March 2012. The trajectories are color-coded with altitude. The time is given in UTC. The ascent and descent time stamps correspond to times when the balloon passed an altitude of 15 km. The burst altitude is localized using a "◯" marker.

applied for the 10–11 February 2013 flight for which no shift remains. In the case of 13 March 2012, a (188 ± 7) m altitude difference is still observed between Pico-SDLA and FLASH water vapor mixing ratio profiles. Although the origin of the shift is not fully understood, one possible explanation is an initialization on FLASH or COBALD error at launch time. Because the Pico-SDLA and the E-track iridium GPS measurements agree to $\pm$20 m between the CPT and 21.3 km, this excludes an error coming from Pico-SDLA GPS altitude measurements. In Fig. 4, a 188 m shift was applied to the FLASH profile. This shift was determined to maximize the correlation coefficient between both profiles. We emphasize that the 13 March 2012 case was the only one where such a high difference in altitude was observed.

Table 1 gives the mean difference between the Pico-SDLA and FLASH descent profiles for the 13 March 2012 flight within three different altitude ranges: 15 to 21.3 km, CPT to 21.3 km and TTL upper level to 21.3 km. Applying the 188 m shift leads to a mean mixing ratio difference of (0.02 ± 0.21) ppmv between 15 and 21.3 km between descent profiles. In this case, Pico-SDLA H_2O is dryer by 0.02 ppmv. Considering the mean mixing ratio, around 4.3 ppmv, the relative difference represents $\sim 0.5\,\%$ (with 1σ standard deviation of 4.6 %). Restricting our comparison to above the CPT, the mean difference is then (0.06 ± 0.18) ppmv (with 1σ standard deviation of 4.2 %). Then, if we consider only the altitude range above the TTL, the mean difference is (0.02 ± 0.16) ppmv (with 1σ standard deviation of 3.7 %). This shows the excellent agreement between the FLASH and Pico-SDLA measurements, which were always within instrumental uncertainties despite the fact that both instruments were flown 3 h apart.

This profile comparison showed identical structures (at 18.1 and 18.7 km of altitude) and mostly with a similar am-

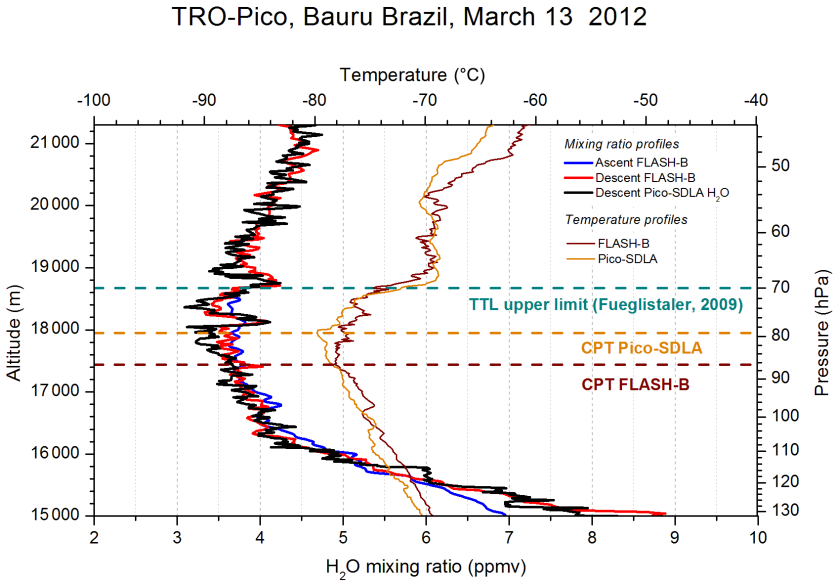

Figure 4. Comparison of water vapor in situ measurements from Pico-SDLA H_2O and FLASH-B hygrometers in the TTL and lower stratosphere for the flight on 13 March 2012. The descent water vapor vertical profile of Pico-SDLA is represented by a solid black line. The ascent and descent water vapor profiles from FLASH-B are shown in solid blue and red lines, respectively. The temperature profiles from Pico-SDLA and FLASH are shown in solid orange and brown lines. The CPT altitude is given by the orange and brown dashed lines for Pico-SDLA and FLASH, respectively. The upper boundary of the TTL is shown by the green dashed line.

Table 1. Mean differences between water vapor descent measurements from Pico-SDLA and FLASH-B on 13 March 2012 within three altitude ranges: 15 to 21.3 km, CPT to 21.3 km and TTL upper level to 21.3 km.

Date of flight	15–21.3 km	CPT–21.3 km	TTL upper level–21.3 km
13 Mar 2012	(0.02 ± 0.21) ppmv	(0.06 ± 0.18) ppmv	(0.02 ± 0.16) ppmv

plitude. Also, the altitude ranges of these structures are very close. The local maximum at 18.1 km (76.6 hPa) stands out with a mixing ratio of 4.09 ppmv in both Pico-SDLA and FLASH measurements (Fig. 4). The structure is a little bit thicker for Pico-SDLA (300 m) than for FLASH (200 m). Also, besides the maximum value being identical for both instruments, the amplitude of the water vapor enhancement is slightly higher for Pico-SDLA (about 0.8 ppmv) whereas FLASH-B shows a 0.65 ppmv enhancement. An air-mass trajectory analysis by Khaykin et al. (2013b) shows that this enhancement is caused by a hydration from overshooting convection, which is about 65 km away from the balloons. The differences in the amplitude of the signal by both instruments can easily be explained by the difference of time of the flights with respect to very local/short duration process. As a result, the instruments cannot sample the same process amplitude. Figure 5 shows the trajectory of both balloons, highlighting the relatively close trajectories which are slightly shifted in space. This helps account for the slight differences between the two profiles. Investigating another large water vapor enhancement at 18.7 km (69 hPa), both instruments measure the same local maximum of 4.19 ppmv. Both the vertical amplitude of the signal (500 m) and the amplitude of the enhancement based on the difference between the bottom of this layer and the local maximum are very similar ~ 1 ppmv. Khaykin et al. (2013b) show that this enhancement is due to large-scale mid-latitude air intrusion, bringing higher mixing ratios of water into the tropical regions. However, it should be noted that the shape of this enhancement is sharper for Pico-SDLA than for FLASH-B. No significant patterns are highlighted above this layer (~ 19 km, 65 hPa) and both instruments report very similar mixing ratios.

4.3 10–11 February 2013

Figure 5 shows the balloon trajectories of both instruments. On this plot we show the descent trajectory of Pico-SDLA and both the ascent and descent trajectory of FLASH-B wherever the ascent measurements of FLASH can be considered. Like for 13 March 2012, the altitude of the trajectories is color-coded. For both instrument trajectories, the time is indicated in UTC. The ascent of Pico-SDLA lasted 1 h 41 min followed by a float of 7 min at 27.4 km (18 hPa) before a 37 min long descent. The ascent of FLASH-B lasted

Table 2. Mean differences between water vapor descent measurements from Pico-SDLA and FLASH-B on 10 and 11 February 2013 within three altitude ranges: 15 to 23 km, CPT to 23 km and TTL upper level to 23 km.

Date of flight	15–23 km	CPT–23 km	TTL upper level–23 km
10–11 Feb 2013	(0.08 ± 0.39) ppmv	(-0.13 ± 0.15) ppmv	(-0.11 ± 0.13) ppmv

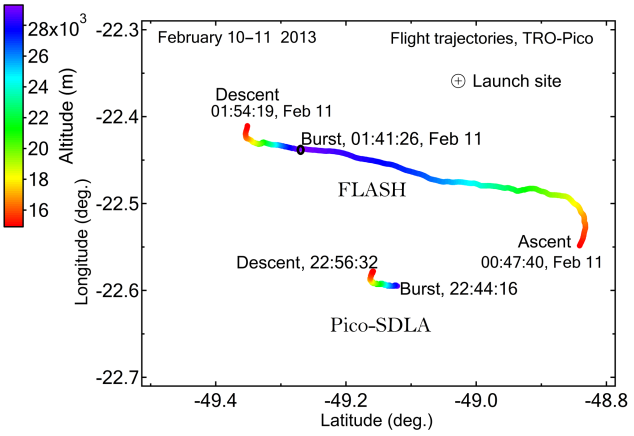

Figure 5. Balloon trajectories of Pico-SDLA and FLASH flights on 10 and 11 February 2013. The trajectories are color-coded with altitude. The time is given in UTC. The ascent and descent time stamps correspond to the times when the balloon passed an altitude of 15 km. The burst altitude is localized using a "◯" marker.

1 h 31 min followed by a descent of 47 min. The maximum altitude reached by the balloon was 28.75 km. We can see in Fig. 5 that Pico-SDLA flew 25 km south of FLASH-B, which resulted in some small differences in the observed water vapor enhancements.

In the case of Pico-SDLA, we use the water vapor measurements below 23 km (33 hPa) because a small outgassing effect (~ 0.4 ppmv) is observed above this height. The balloon carrying the FLASH-B flight train is much smaller than the 1500 m^3 balloon used for Pico-SDLA. Since the smaller balloon reduces the amount of water vapor outgassing, we are able to consider the FLASH-B ascent profile up to approximately 18 km (77 hPa) of altitude, above which a small outgassing effect starts to be observed. This leads to the comparison shown in Fig. 6. In this figure, we present in situ water vapor measurements between 15 km (131 hPa) and 23 km (34 hPa) from Pico-SDLA H_2O and FLASH-B. The upper boundary of the TTL corresponds to an altitude of 18.8 km (70 hPa level) and is shown by a green dotted line. In the case of Pico-SDLA, the CPT is 16.63 km ($P = 99.9$ hPa, $T = -74.15$ °C) and for FLASH it is 16.98 km ($P = 92.2$ hPa, $T = -75.2$ °C). The difference between the CPT altitudes from Pico-SDLA and FLASH observed for the two flights can be attributed to three different factors: a natural temporal and spatial temperature variability in the TTL, the measurement uncertainties and how the temperature structures are resolved. For both flights the CPT is not well pronounced, which makes its determination difficult. However, even though both CPT values are different by ~ 300 m, the overall temperature profile is similar and the CPT altitudes are comparable.

Analyzing the profile comparison in more detail, we find that the main structures are well captured by both instruments above and around the CPT, although the amplitude of the local maxima/minima sometimes varies slightly. Three water vapor enhancement structures appear on the descent profile of Pico-SDLA at altitudes of 16.5 km (102 hPa), 17.2 km (90.7 hPa) and 18 km (78.5 hPa). The structure at 16.5 km is captured by FLASH during the ascent but not during the descent and is shifted downwards by about 90 m in altitude compared to the Pico-SDLA. The amplitude of the enhancement is, in the case of FLASH, about 0.5 ppmv and around 0.68 ppmv for the Pico-SDLA. During the descent, the structure at 17.2 km shifted upward by 50 m as captured by FLASH-B. The ascent profile of FLASH-B also shows the structure at the same altitude but the noise amplitude is larger rendering the structure much harder to distinguish. For both instruments, the amplitude of the enhancement is similar but the structure is slightly thicker in the case of FLASH (nominally 560 m) instead of 500 m for Pico-SDLA. The structure at 18 km was captured by FLASH-B during the ascent and during the descent. The ascent profile of FLASH-B shows only one structure at 18 km whereas the descent profile shows two structures at 17.8 and 18.1 km of 280 and 300 m thickness, respectively. Because of a small amount of outgassing, the ascent profile of FLASH-B above 17.7 km cannot be considered for analysis. Nevertheless, structures are visible. The small altitude difference is of the same order of magnitude as the GPS height uncertainty. It also must be considered that the hygrometers did not fly at exactly the same time.

The mean difference between the Pico-SDLA and FLASH descent measurements is given in Table 2 within several altitude ranges. Over the altitude range between 15 and 18 km, comparison between the ascent of FLASH-B and the descent of Pico-SDLA leads to a mean difference of (0.13 ± 0.33) ppmv. In the altitude range between 15 and 23 km, the comparison between the descent profiles of both instruments yields a mean mixing ratio difference of (0.08 ± 0.39) ppmv. FLASH-B is dryer than Pico-SDLA by 0.08 ppmv at the descent. Considering the 4.1 ppmv mean mixing ratio over the 15 to 23 km altitude range, the differences observed correspond to 1.9 % (with a 1σ standard deviation of 9.5 %). Restricting our comparison to above the

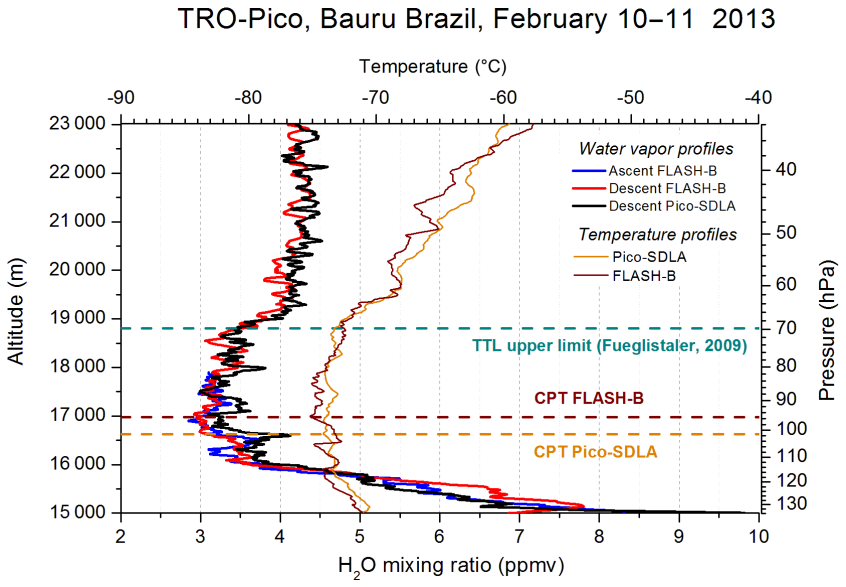

Figure 6. Comparison of water vapor in situ measurements from Pico-SDLA H_2O and FLASH-B hygrometers in the TTL and lower stratosphere for the flight of 10 February 2013. The descent water vapor vertical profile of Pico-SDLA is represented by the solid black line. The ascent and descent water vapor profiles from FLASH-B are shown as solid blue and red lines, respectively. The temperature profiles from Pico-SDLA and FLASH are shown in orange and brown lines. The CPT altitude is given by the orange and brown dashed lines for Pico-SDLA and FLASH, respectively. The upper boundary of the TTL is shown is given by the green dashed line.

CPT, the mean difference is then (-0.13 ± 0.15) ppmv (1σ standard deviation of 3.7 %). We clearly see the impact of the humidity variability in the lower TTL region on the statistical results. The strong humidity variability induces a larger standard deviation and therefore less precise results. To obtain a purely stratospheric comparison, it is generally better to consider data above the TTL upper limit (i.e., 19 km). In this case, the mean difference is then (-0.11 ± 0.13) ppmv (1σ standard deviation of 3.2 %). We notice that the above CPT and the above TTL statistical results are not very different. Since the maximum altitude usable in this case is 23 km, we can consider the data above the CPT to test the consistency of Pico-SDLA and FLASH measurements. Then, we obtain a larger altitude range for comparison. Although both instruments were flown 3 h apart, the measurements are in good agreement.

5 Pico-SDLA/FLASH-B correlation

Figure 7 shows a scatter plot comparison of Pico-SDLA versus FLASH water vapor measurements for the flights on 13 March 2012 and 10 February 2013. The data are color-coded by pressure in the altitude range from the CPT altitude up to the altitude free of outgassing for each flight. A linear fit of the Pico-SDLA versus FLASH data is shown as a solid line and the equations of the fits are given. The bias ($\hat{b}$) has been calculated using the following equation:

$$\hat{b} = \sum_{i=1}^{n} \frac{\text{mix.ratio}_i\,(\text{P-SDLA}) - \text{mix.ratio}_i\,(\text{FLASH})}{n}. \qquad (1)$$

Here, n represents the number of measurements. For these two flights, between the CPT and the maximum altitude usable, the maximum bias visible is ~ 0.12 ppmv (10–11 February 2013 flight). For the 13 March 2012 flight, this bias is ~ -0.06 ppmv. Both biases are the same amplitude of those in Weinstock et al. (2009), obtained from coinciding flights. Since the bias varies from one flight to the other, no systematic bias has been demonstrated between Pico-SDLA and FLASH.

We have calculated the Pearson's r coefficient from 15 km and from the CPT altitude. This coefficient is calculated from the linear least-squares fitting of the scatter plot data and represents the correlation coefficient.

For the 10 February 2013 flight results, $r = 0.92$ for the 15 to 23 km range and $r = 0.95$ for the CPT (16.7 to 23 km) range. In this case, the water vapor enhancements at 17.2 and 18 km, which are seen by Pico-SDLA but not by FLASH, and the humidity variability in the lower TTL region have a significant impact on the correlation.

In the case of the 13 March 2012 flights, the correlation coefficient is mainly affected by the two large water vapor enhancements observed at 18.1 and 18.7 km which do not have exactly the same thickness and amplitude. Within 15 to 21.2 km, the r is equal to 0.98. Surprisingly, r decreases to 0.89 between the CPT (17.7 km) and 21.2 km. The statistical weight of the two structures at 18.1 and 18.7 km is larger in the calculation when only altitudes above CPT are considered.

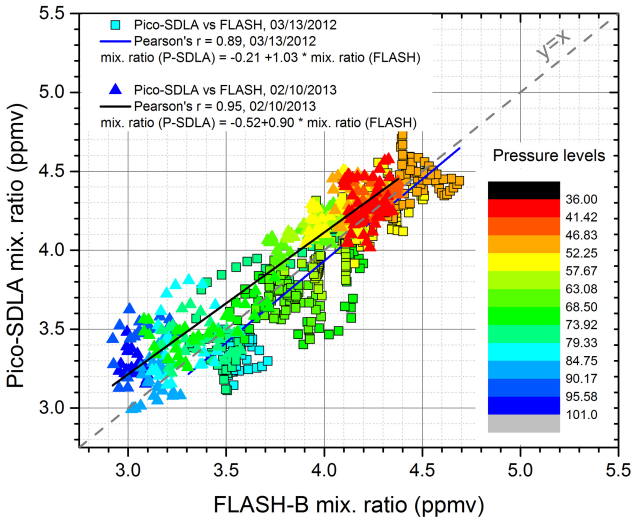

Figure 7. Scatter plot comparison of Pico-SDLA versus FLASH water vapor measurements between the CPT and the free-of-outgassing altitude (21.3 km on 13 March 2012 and 23 km on 10 February 2013). The linear fit of the data is represented with solid blue and black lines for the 13 March 2012 and 10 February 2013 flights, respectively. The data are color mapped by the pressure.

Because the two sensors did not fly at the same time, the correlation is strongly affected by the variability in the water vapor enhancement structures shown by the two different hygrometers. This effect is clearly visible through the changes in r between the two altitude ranges. In the case of 13 March 2012 r is strongly affected by the two enhancement structures (one is even present above the TTL upper limit). Despite the evident impact of the vertical structures on the results, the present comparison exhibits some of the best agreement found in the literature for studies realized from coincident flights (Weinstock et al., 2009; Khaykin et al., 2013a). In each case, the water vapor enhancements are of much larger amplitude than the difference between the two instruments. FLASH and Pico-SDLA are therefore able to see, with good accuracy, the impact of dynamical process on water vapor concentrations.

6 Summary and conclusions

This work compares in situ water vapor measurements from two hygrometers: Pico-SDLA H_2O and FLASH-B, obtained during the TRO-Pico balloon campaign held in Brazil between 2012 and 2013. It serves as the basis for a future paper (S. M. Khaykin, personal communication, 2015), centered on the meteorological analysis of the measurements.

The hygrometers were deployed on 13 March 2012 and 10 February 2013 when an overshooting convection event was observed in the vicinity of the flight paths. The impact of overshoots on water vapor mixing ratios is visible on 13 March 2012 by the presence of two vertical structures at 18.1 and 18.7 km. A detailed analysis of this profile will be given in the forthcoming paper (S. M. Khaykin, personal communication, 2015).

The water vapor profiles were compared within two altitude ranges: above 15 km and above the CPT. The comparison above 15 km shows larger deviations (up to 9.5 % ≡ 0.39 ppmv) than those above the CPT (around 4 % ≡ 0.16 ppmv) because of humidity variability in the uppermost troposphere. On 13 March 2012 and 10 February 2013, the mean difference of mixing ratios is 0.5 % ((0.02 ± 0.21) ppmv) and 1.9 % ((0.08 ± 0.39) ppmv), respectively, above the CPT altitude, differences which are well below both instrument uncertainties. The differences are then much lower than the amplitude of the water vapor enhancements (between 0.5 and 0.8 ppmv), permitting us to reliably detect these overshoot signatures. Because the hygrometers were not flown at the same time, the humidity variability through the TTL had an important impact on the correlation coefficient and on the mixing ratio differences between the two instruments. Nevertheless, the differences observed in this study are well below the majority of in situ comparisons in the TTL and constitute one of the best intercomparison results by comparison to the work of Weinstock et al. (2009) and Khaykin et al. (2013a). In these previous studies, the mixing ratio differences for in situ measurements ranged between 0.8 and 5 % and were obtained for coincident flights. In the context where persistently large disagreements exist between in situ measurements, the present work shows that Pico-SDLA H_2O and FLASH-B are suitable for accurate in situ water vapor measurements over a variety of conditions, such as those including strong convection and high vertical speed. Furthermore, given the small differences observed among the profiles of each instrument, it can be concluded that the H_2O data provided by the TRO-Pico campaign made of Pico-SDLA and FLASH-B measurements are mutually consistent. The compactness of these instruments permits their deployment under small weather balloons and therefore allows frequent soundings of the upper troposphere and lower stratosphere to be performed.

Acknowledgements. This work and the TRO-Pico project were supported by Agence Nationale de la Recherche (ANR) under contract ANR-2010-BLAN-609-01 and by the region Champagne-Ardenne in France. The authors are grateful for the logistical and infrastructural support provided by IPMet/UNESP under a collaborative agreement with the French CNRS. We also thank IPMet's technicians, Hermes França, Bruno Biazon and Demilson Quintão, for their assistance during the TRO-Pico campaigns and Joseph T. Hodges from NIST for his greatly appreciated help reviewing this paper.

Edited by: M. von Hobe

References

Bertaux, J. L. and Delannoy, A. : Premières mesures stratosphériques par un hygromètre à fluorescence ultra-violette, C. R. Acad. Sci. Paris, 286, 191–194, 1978.

Berthet, G., Renard, J.-B., Ghysels, M., Durry, G., Gaubicher, B., and Amarouche, N. : Balloon-borne observations of mid-latitude stratospheric water vapour at two launching sites: comparisons with HALOE and MLS satellite data, J. Atmos. Chem., 70, 197–219, 2013.

Boone, C. D., Walker, K. A., and Bernath, P. F.: Speed-dependent Voigt profile for water vapor lines in infrared remote sensing applications, J. Quant. Spectrosc. Ra., 105, 525–532, 2007.

Bower, C. A. and Fitzgibbon, J. J.: National Weather Service In-situ Radiation Temperature Correction for Radiosonde Replacement System GPS Radiosondes, Eighth Symposium on Integrated Observing and Assimilation Systems for Atmosphere, Oceans, and Land Surface, Seattle, USA, 10 January 2004, 3.1, available at: https://ams.confex.com/ams/84Annual/techprogram/paper_74046.htm (last access: 17 December 2015), 2004.

Brabec, M., Wienhold, F. G., Luo, B. P., Vömel, H., Immler, F., Steiner, P., Hausammann, E., Weers, U., and Peter, T.: Particle backscatter and relative humidity measured across cirrus clouds and comparison with microphysical cirrus modelling, Atmos. Chem. Phys., 12, 9135–9148, doi:10.5194/acp-12-9135-2012, 2012.

Dicke, R. H.: The effect of collisions upon the Doppler width of spectral lines, Phys. Rev., 89, 472–473, 1953.

Durry, G., Amarouche, N., Joly, L., Liu, X., Parvitte, B., and Zeninari, V. : Laser diode spectroscopy of H_2O at 2.63 µm for atmospheric applications, Appl. Phys. B, 90, 573–580, 2008.

Dvorstov, V. L. and Solomon, S.: Response of the stratospheric temperatures and ozone to past and future increases in stratospheric humidity, J. Geophys. Res., 106, 7505–7514, 2001.

Forster, P. M. F. and Shine, K.,P.: Assessing the climate impact of trends in stratospheric water vapor, Geophys. Res. Lett., 29, 10-1–10-4, 2002.

Fueglistaler, S., Dessler, A., Dunkerton, T., Folkins, I., Fu, Q., and Mote, P., W. : Tropical tropopause layer, Rev. Geophys., 47, RG1004, doi:10.1029/2008RG000267, 2009.

Ghysels, M., Gomez, L., Cousin, J., Amarouche, N., Jost, H., and Durry, G.: Spectroscopy of CH_4 with a difference-frequency generation laser at 3.3 microns for atmospheric applications, Appl. Phys. B, 104, 989–1000, 2011.

Herman, R. L., Drdla, K., Spackman, J. R., Hurst, D. F., Popp, P. J., Webster, C. R., Romashkin, P. A., Elkins, J. W., Weinstock, E. M., Gandrud, B. W., Toon, G. C., Schoeberl, M. R., Jost, H., Atlas, E. L.. and Bui, T. P. : Hydratation, dehydration, and the total hydrogen budget of the 1999/2000 winter Arctic stratosphere, J. Geophys. Res., 107, 2002–2014, 2002.

Holton, J. R., Haynes, P. H., McIntyre, M. E., Douglass, A. R., Rood, R. B., and Pfister, L. :Stratosphere-troposphere exchange. Rev. Geophys., 33, 403–439, 1995.

Hurst, D. F., Hall, E. G., Jordan, A. F., Miloshevich, L. M., Whiteman, D. N., Leblanc, T., Walsh, D., Vömel, H., and Oltmans, S. J.: Comparisons of temperature, pressure and humidity measurements by balloon-borne radiosondes and frost point hygrometers during MOHAVE-2009, Atmos. Meas. Tech., 4, 2777–2793, doi:10.5194/amt-4-2777-2011, 2011.

Immler, F. J., Dykema, J., Gardiner, T., Whiteman, D. N., Thorne, P. W., and Vömel, H.: Reference Quality Upper-Air Measurements: guidance for developing GRUAN data products, Atmos. Meas. Tech., 3, 1217–1231, doi:10.5194/amt-3-1217-2010, 2010.

Jensen, E. J., Smith, J. B., Pfister, L., Pittman, J. V., Weinstock, E. M., Sayres, D. S., Herman, R. L., Troy, R. F., Rosenlof, K., Thompson, T. L., Fridlind, A. M., Hudson, P. K., Cziczo, D. J., Heymsfield, A. J., Schmitt, C., and Wilson, J. C.: Ice supersaturations exceeding 100 % at the cold tropical tropopause: implications for cirrus formation and dehydration, Atmos. Chem. Phys., 5, 851–862, doi:10.5194/acp-5-851-2005, 2005.

Jensen, E. J., Pfister, L., Bui, T. V., Lawson, P., Baker, B., Mo, Q., Baumgardner, D., Weinstock, E. M., Smith, J. B., Moyer, E. J., Hanisco, T. F., Sayres, D. S., Clair, J. M. St., Alexander, M. J., Toon, O. B., and Smith, J. A.: Formation of large ($\sim$ 100 µm) ice crystals near the tropical tropopause, Atmos. Chem. Phys., 8, 1621–1633, doi:10.5194/acp-8-1621-2008, 2008.

Khaykin, S. M., Engel, I., Vömel, H., Formanyuk, I. M., Kivi, R., Korshunov, L. I., Krämer, M., Lykov, A. D., Meier, S., Naebert, T., Pitts, M. C., Santee, M. L., Spelten, N., Wienhold, F. G., Yushkov, V. A., and Peter, T.: Arctic stratospheric dehydration – Part 1: Unprecedented observation of vertical redistribution of water, Atmos. Chem. Phys., 13, 11503–11517, doi:10.5194/acp-13-11503-2013, 2013a.

Khaykin, S. M., Pommereau, J.-P., Riviere, E., Ghysels, M., Amarouche, N., Ploegner, F., Vernier, J.-P., Wienhold, F. G., and Held, G.: Vertical and horizontal transport of water vapour and aerosol in the tropical stratosphere from high-resolution balloon-borne observations, Poster session presented at the EGU general assembly 2013, 7–12 April 2013, Vienna, Austria, EGU2013-4813, 2013b.

Kim, J. and Son, S.-W.: Tropical Cold-Point Tropopause: Climatology, Seasonal Cycle and Intraseasonal Variability Derived from COSMIC GPS Radio Occultation Measurements, J. Climate, 25, 5343–5360, 2012.

Kindel, B. C., Pilewskie, P., Schmidt, K. S., Thornberry, T., Rollins, A., and Bui, T.: Upper-troposphere and lower-stratosphere water vapor retrievals from the 1400 and 1900 nm water vapor bands, Atmos. Meas. Tech., 8, 1147–1156, doi:10.5194/amt-8-1147-2015, 2015.

Kley, D. and Stone, E. J.: Measurements of water vapor in the stratosphere by photodissociation with Ly α (1216 Å) light, Rev. Sci. Instrum., 49, 691–697, 1978.

Kley, D., Russell III, J. M., and Phillips, C.: SPARC assessment of upper tropospheric and stratospheric water vapour, World Meteorol. Org., Geneva, Switzerland, 2000.

Loewenstein, M., Jost, H., Grose, J., Eilers, J., Lynch, D., Jensen, S., and Marmie, J.: Argus: a new instrument for the measurement of the stratospheric dynamical tracers, N_2O and CH_4, Spectrochim. Acta A, 58, 2329–2347, 2002.

Mastenbrook, H. J.: Water vapor distribution in the stratosphere and High troposphere, J. Atmos. Sci., 25, 299–311, 1968.

Mote, P. W., Rosenlof, K. H., McIntyre, M. E., Carr, E. S., Gille, J. C., Holton, J. R., Kinnersley, J. S., Pumphrey, H. C., Russell III, J. M., and Waters, J. W.: An atmospheric tape recorder : the imprint of tropical tropopause temperatures on stratospheric water vapor, J. Geophys. Res., 101, 3989–4006, 1996.

Nash, J., Oakley, T., Vömel, H., and Wei, L. I.: WMO intercomparison of high quality radiosonde systems, Instruments and ob-

serving methods report No. 107, Yangjiang, China, 12 July–3 August 2010, Chairperson, Publications Board,World Meteorological Organization (WMO), 2011.

Oltmans, S. J., Vömel, H., Hofmann, D. J., Rosenlof, K. H., and Kley, D.: The increase in stratosphericwater vapor from balloonborne, frostpoint hygrometer measurements at Washington D.C., and Boulder, Colorado, Geophys. Res. Lett., 27, 3453–3456, 2000.

Randel, W. J. and Jensen, E. J.: Physical processes in the tropical tropopause layer and their roles in a changing climate, Nat. Geosci., 6, 196–176, 2013.

Rautian, S. G. and Sobel'man, I. I. : The effect of collisions on the Doppler broadening of spectral lines, Sov. Phys. Uspekhi, 9, 701–716, 1967.

Read, W. G., Lambert, A., Bacmeister, J., Cofield, R., E., Christensen, L. E., Cuddy, D. T., Daffer, W. H., Drouin, B. J., Fetzer, E., Froidevaux, L., Fuller, R., Herman, R., Jarnot, R. F., Jiang, J. H., Jiang, Y. B., Kelly, K., Knosp, B. W., Kovalenko, L. J., Livesey, N. J., Liu, H.-C., Manney, G. L., Pickett, H. M., Pumphrey, H. C., Rosenlof, K. H., Sabounchi, X., Santee, M. L., Schwartz, M. J., Snyder, W. V., Stek, P. C., Su, H., Takacs, L. L., Thurstans, R. P., Vömel, H., Wagner, P. A., Waters, J. W., Webster, C. R., Weinstock, E. M., and Wu, D. L. : Aura Microwave Limb Sounder upper tropospheric and lower stratospheric H_2O and relative humidity with respect to ice validation, J. Geophys. Res., 112, D24S35, doi:10.1029/2007JD008752, 2007.

Renard, J.-B., Dulac, F., Berthet, G., Lurton, T., Vignelles, D., Jégou, F., Tonnelier, T., Thaury, C., Jeannot, M., Couté, B., Akiki, R., Verdier, N., Mallet, M., Gensdarmes, F., Charpentier, P., Duverger, V., Dupont, J.-C., Mesmin, S., Elias, T., Crenn, V., Sciare, J., Giacomoni, J., Gobbi, M., Hamonou, E., Olafsson, H., Dagsson-Waldhauserova, P., Camy-Peyret, C., Mazel, C., Décamps, T., Piringer, M., Surcin, J., and Daugeron, D.: LOAC: a small aerosol optical counter/sizer for ground-based and balloon measurements of the size distribution and nature of atmospheric particles – Part 1: Principle of measurements and instrument evaluation, Atmos. Meas. Tech. Discuss., 8, 9993–10056, doi:10.5194/amtd-8-9993-2015, 2015.

Riese, M., Ploeger, F., Rap, A., Vogel, B., Konopka, P., Dameris, M., and Forster, P. Impact of uncertainties in atmospheric mixing on simulated UTLS composition and related radiative effects, J. Geophys. Res.-Atmos., 117, D16305, doi:10.1029/2012JD017751, 2012.

Rollins, A. W., Thornberry, T. D., Gao, R. S., Smith, J. B.,Sayres, D. S., Sargent, M. R., Schiller, C., Krämer, M., Spelten, N., Hurst, D. F., Jordan, A. F., Hall, E. G., Vömel, H., Diskin, G. S.,Podolske, J. R., Christensen, L. E., Rosenlof, K. H., Jensen, E. J., and Fahey, D. W.: Evaluation of UT/LS hygrometer accuracy by intercomparison during the NASA MACPEX mission, J. Geophys. Res. Atmos., 119, 1915–1935, doi:10.1002/2013JD020817, 2014.

Rosenlof, K. H., Oltmans, S. J., Kley, D., Russel III, J. M., Chiou, E. W., Chu, W. P., Johnson, D. G., Kelly, K. K., Michelsen, H. A., Nedoluha, G. E., Remsberg, E. E., Toon, G. C., and McCormick, M. P.: Stratospheric water vaporincreases over the past half-century, Geophys. Res. Lett., 28, 1195–1198, 2001.

Rothman, L. S., Gordon, I. E., Babikov, Y., Barbe, A., Chris Benner, D., Bernath, P. F., Birk, M., Bizzocchi, L., Boudon, V., Brown, L. R., Campargue, A., Chance, K., Cohen, E. A, Coudert, L. H., Devi, V. M., Drouin, B. J., Fayt, A., Flaud, J.-M., Gamache, R. R., Harrison, J. J.., Hartmann, J.-M., Hill, C., Hodges, J. T., Jacquemart, D., Jolly, A., Lamouroux, J., Le Roy, R., J., Li, G., Long, D. A., Lyulin, O. M., Mackie, C. J., Massie, S. T., Mikhailenko, S., Müller, H. S., P., Naumenko, O. V., Nikitin, A. V., Orphal, J., Perevalov, V., Perrin, A., Polovtseva, E. R., Richard, C., Smith, M. A. H., Starikova, E., Sung, K., Tashkun, S., Tennyson, J., Toon, G. C., Tyuterev, V. G., and Wagner, G.: The HITRAN 2012 molecular spectroscopic database, J. Quant. Spectrosc. Ra., 130, 4–50, 2013.

Shindell, D. J.: Climate and ozone response to increased stratospheric water vapor, Geophys. Res. Lett., 28, 1551–1554, 2001.

Shindell, D. T., Rind, D., and Lonergan, P. : Increased polar stratospheric ozone losses and delayed eventual recovery owing to increasing greenhouse-gas concentrations, Nature, 392, 589–592, 1998.

Solomon, S., Rosenlof, K., H., Portmann, R., W., Daniel, J. S., Davis, S. M., Sanford, T. J., and Plattner, G.-K.: Contributions of stratospheric water vapor to decadal changes in the rate of global warming, Science, 327, 1219–1223, 2010.

Tran, H., Bermejo, D., Domenech, J.-L., Joubert, P., Gamache, R. R., and Hartmann, J.-M. : Collisional parameters of H2O lines: Velocity effects on the line-shape, J. Quant. Spectrosc. Ra., 108, 126–145, 2007.

Vömel, H., Oltmans, S. J., Johnson, B. J., Shiotani, M., Fujiwara, M., Nishi, N., Agama, M., Cornejo, J., Paredes, F., and Enriquez, H. : Balloon-borne observations of water vapor and ozone tropical upper troposphere and lower stratosphere, J. Geophys. Res., 107, 4210, doi:10.1029/2001JD000707, 2002.

Vömel, H., David, D. E., and Smith, K.: Accuracy of tropospheric and stratospheric water vapor measurements by the cryogenic frost point hygrometer : Instrumental details and observations, J. Geophys. Res., 112, D08305, doi:10.1029/2006JD007224, 2007a.

Vömel, H., Yushkov, V., Khaykin, V, Korshunov, V., Kyrö, E., and Kivi, R.: Intercomparisons of stratospheric water vapor sensors: FLASH-B and NOAA/CMDL frost-point hygrometer, J. Atmos. Ocean. Tech., 24, 941–952, doi:10.1175/JTECH2007.1, 2007b.

Weinstock, E. M., Smith, J. B., Sayres, D. S., Pittman, J. V., Spackman, J. R., Hintsa, E. J., Hanisco, T. F., Moyer, E. J., St. Clair, J. M., Sargent, M. R., and Anderson, J. G.: Validation of the Harvard Lyman-α in situ water vapor instrument: implications for the mechanisms that control stratospheric water vapor, J. Geophys. Res., 114, D23301, doi:10.1029/2009JD012427, 2009.

Yushkov, V., Astakhov V., and Merkulov, S.: Optical balloon hygrometer for upper-troposphere and stratosphere water vapor measurements, in: Proceedings SPIE 3501, Optical Remote Sensing of the Atmosphere and Clouds, Beijing, China, 14 September 1998, 439–445, 1998.

Zander, R.: Moisture contamination at altitude by balloon and associate equipment, J. Geophys. Res., 71, 3775–3778, 1966.